

Star-formation in the HI bridge between M81 and M82¹

D. F. de Mello^{2,3,4}

L. J. Smith^{5,6,7}, E. Sabbi⁵, J.S. Gallagher⁸, M. Mountain⁵ & D.R. Harbeck⁸

ABSTRACT

We present multi-wavelength observations of stellar features in the HI tidal bridge connecting M81 and M82 in the region called Arp's Loop. We identify eight young star-forming regions from Galaxy Evolution Explorer ultraviolet observations. Four of these objects are also detected at H α . We determine the basic star formation history of Arp's Loop using F475W and F814W images obtained with the Advanced Camera for Surveys on board the Hubble Space Telescope. We find both a young (< 10 Myr) and an old (> 1 Gyr) stellar population with a similar spatial distribution and a metallicity $Z \sim 0.004$. We suggest that the old stellar population was formed in the stellar disk of M82 and/or M81 and ejected into the intergalactic medium during a tidal passage (~ 200 – 300 Myr ago), whereas the young UV-bright stars have formed in the tidal debris. The UV luminosities of the eight objects are modest and typical of small clusters or OB associations. The tidal bridge between M81–M82 therefore appears to be intermediate between the very low levels of star formation seen in the Magellanic bridge and actively star-forming tidal tails associated with major galaxy mergers.

¹Based on observations with the NASA/ESA *Hubble Space Telescope*, obtained from the Data Archive at the Space Telescope Science Institute, which is operated by AURA, Inc., under NASA contract NAS5–26555. These observations are associated with program #10915.

²Observational Cosmology Laboratory, Code 665, Goddard Space Flight Center, Greenbelt, MD 20771

³Catholic University of America Washington, DC 20064

⁴Johns Hopkins University, Baltimore, MD 21218

⁵Space Telescope Science Institute, 3700 San Martin Dr., Baltimore, MD 21218

⁶ESA Space Telescope Operations Division

⁷Department of Physics and Astronomy, University College London, Gower Street, London WC1E 6BT, UK

⁸Department of Astronomy, University of Wisconsin-Madison, 475 North Charter Street, Madison, WI 53706

Subject headings: galaxies: general — galaxies: evolution — galaxies: interactions — galaxies: individual (M81, M82)

1. Introduction

The M81 group contains three major closely interacting galaxies: M81, M82 and NGC 3077. Studies of this triple system at radio wavelengths have shown an extremely disturbed HI distribution with tidal bridges connecting the three galaxies (e.g. Gottesman & Weliachew 1975; van der Hulst 1979; Appleton, Davies & Stephenson 1981; Yun, Ho & Lo 1994). Within the tidal bridges, HI knots with optical counterparts are seen. The most prominent of these to the east/north-east of M81 are Holmberg IX and Arp’s Loop or A0952+69 (Arp 1965). It has been suggested (e.g. Boyce et al. 2001) that these are forming tidal dwarf galaxies. Numerical simulations of the system by Yun (1999) can successfully reproduce the the HI tidal debris if the closest approaches of M82 and NGC 3077 to M81 took place 220 and 280 Myr ago respectively. Arp’s loop, the topic of this paper, occurs at the intersection of the three tidal streamers in the simulation of Yun (1999) who gives an HI mass of $2.6 \times 10^8 M_{\odot}$. Sun et al. (2005) present very deep wide-field optical continuum images of the M81/M82 galaxy group, and show that groups of young stars are distributed across the entire region between the two galaxies.

Although tidal tails usually have blue optical colors (e.g. Schombert et al. 1990), it is not clear whether these colors are due to tidally-disrupted stellar disk material or active star formation in the tails. Recently, ultraviolet (UV) imaging obtained with the Galaxy Evolution Explorer (GALEX) satellite has shown that regions of bright UV emission, containing recently formed stars, correlate well with regions of high HI column density in tidal tails (e.g. Hibbard et al. 2005; Neff et al. 2005). These findings suggest that the combination of UV and HI data provides a powerful technique for identifying and studying star formation in the intergalactic medium (IGM) between interacting galaxies. This topic is of importance for earlier epochs in the universe because galaxy interactions, and thus tidal tails were more common, leading to a higher star formation rate in the IGM. This may well have implications for the enrichment of the IGM; Ryan-Weber et al. (2004) have shown that stars forming in the IGM offer a viable alternative to galactic wind enrichment on large scales.

We have thus started a study of star formation in the IGM of the M81 galaxy group with the overall aim of elucidating the importance of this mode of star formation. We present

results for Arp’s loop in this paper and for Holmberg IX in Sabbi et al. (2007). Arp’s loop is located 17 arcmin north-east of M81 and its composition was first discussed by Efremov et al. (1986). They resolved the ring-like structure into blue diffuse and star-like objects which they interpreted as young star clusters and associations. Makarova et al. (2002) investigated the stellar population of Arp’s loop using photometry obtained with the Wide Field and Planetary Camera 2 (WFPC2) on board the Hubble Space Telescope (HST). They were unable to clarify the evolutionary nature of Arp’s loop because of photometric limitations and WFPC2’s small field of view. They find evidence for: enhanced star formation between 20 and 200 Myr ago, coincident with the likely epoch of tidal interactions in the M81 group; intermediate age stars which were either formed prior to the interaction in the Arp’s loop or were torn out of the massive galaxies during the interaction; and also faint stars with ages ≥ 8 Gyr but which were too close to the detection limit for detailed analysis. In this paper, we use multi-wavelength observations, including deep photometry obtained with the Advanced Camera for Surveys (ACS), to resolve the stellar population, and thus determine the evolutionary status of Arp’s loop.

2. The Data

2.1. GALEX, ACS, HI and WIYN

The M81 group was observed with the Galaxy Evolution Explorer (GALEX) mission in the far (FUV: $\lambda_{\text{eff}}=1528\text{\AA}$; $\Delta\lambda_{\text{FUV}}=269\text{\AA}$) and near ultraviolet (NUV: $\lambda_{\text{eff}}=2271\text{\AA}$; $\Delta\lambda_{\text{NUV}}=616\text{\AA}$). We obtained the data from the Multimission Archive at STScI (MAST) as part of the team General Releases. The GALEX field of view is $1^\circ.28$ and $1^\circ.24$ in the FUV and NUV bands, and the pixel scale is $1.5''/\text{pixel}$. The exposure times were 3093s for each band.

Fluxes were calculated using the equations of Morrissey et al. (2005): $m_\lambda = -2.5 \log[F_\lambda/a_\lambda] + b_\lambda$, where $a_{\text{FUV}} = 1.4 \times 10^{-15} \text{ erg s}^{-1} \text{ cm}^{-2} \text{ \AA}^{-1}$, $a_{\text{NUV}}=2.06 \times 10^{-16} \text{ erg s}^{-1} \text{ cm}^{-2} \text{ \AA}^{-1}$, $b_{\text{FUV}}=18.82$ and $b_{\text{NUV}}=20.08$ for FUV and NUV, respectively. Fluxes were multiplied by the effective filter bandpass ($\Delta\lambda_{\text{FUV}}=269\text{\AA}$ and $\Delta\lambda_{\text{NUV}}=616\text{\AA}$) to give units of $\text{erg s}^{-1} \text{ cm}^{-2}$ and luminosities were calculated for a distance of 3.6 Mpc (Freedman et al. 1994).

Figure 1 shows the distribution of the atomic hydrogen in the M81 group of galaxies (Yun, Ho & Lo 1994) on top of the GALEX FUV image. We have identified 8 FUV objects (Fig. 2, Table 1) inside the HI cloud located on the northeast side of the bridge between M81 and M82 and north of Holmberg IX. This region, called concentration II by Yun et

al., is the brightest H I complex in the tidal bridge. It includes Arp’s loop, and may not be a single cohesive feature, containing tidally stripped gas from M81 and M82. Makarova et al. (2002) found 250 stars in the HST/WFPC2 F606W/F814W images of Arp’s loop. However, the WFPC2 observations were centered on the H I concentration and cover only objects #7 and #8, missing the other FUV objects. We searched the HST archive at MAST and found new pointings of the same area but taken with the Wide Field Channel (WFC) of ACS using the F475W and F814W filters and covering a larger field of view (GO 10915: PI Dalcanton). Fig. 3 shows the ACS F475W image where we have plotted the WFPC2 footprint, the GALEX contours, and marked the 8 FUV objects. The high resolution of ACS (0.05”) resolves the FUV objects into hundreds of starlike objects as can be seen in Fig. 4. However, the ACS pointing misses two of the FUV objects (#3 and #4) and part of another object (#1).

We have also obtained an H α image of Arp’s loop with the OPTIC imager at the WIYN¹ 3.5m telescope. The observations were taken with WIYN filter # 13 ($\Delta\lambda = 47 \text{ \AA}$) and a standard Johnson *R* filter for continuum subtraction. OPTIC is a mosaic of two 2kx4k orthogonal transfer CCDs, resulting in a field of view of 9.5’x9.5’. In Fig. 5 we present only an image of chip #2 which was bias-corrected and flat-fielded using IRAF² The two images taken in each filter were combined with cosmic-ray rejection, and the resulting scaled *R*-band image was subtracted from the combined H α image to remove the continuum signal. Our data confirm Karachentsev & Kaisin’s (2007) detection of objects #1, #8, #7, and #3, with #1 being the brightest and #3 the faintest object (see fig.1 in Karachentsev & Kaisin). As shown in Fig. 5, although we have detected the faintest object, we have not detected two of their H α sources which are marked as squares in Fig. 5. This could be due to the different bandwidths, since Karachentsev & Kaisin used a broader filter ($\Delta\lambda = 75 \text{ \AA}$) than ours. H α detections of the FUV sources suggest that these are small H II regions where hot, blue OB stars are emitting ultraviolet radiation.

3. Color-Magnitude Diagram

In order to investigate the stellar content of the FUV objects, we have performed photometry on the two ACS/WFC images. The total exposure times for the fully reduced

¹The WIYN Observatory is a joint facility of the University of Wisconsin-Madison, Indiana University, Yale University, and the National Optical Astronomy Observatories.

²IRAF is distributed by the National Optical Astronomy Observatory, which is operated by AURA, Inc., under cooperative agreement with the National Science Foundation.

and multidrizzled images are 2250 s in the F475W ($\sim B$) band and 2265 s in the F814W ($\sim I$) band respectively. Each image covers an area of $200'' \times 200''$, which corresponds to 3.5×3.5 kpc for the distance of M81. The images were reduced using the standard STScI ACS pipeline CALACS (Pavlovsky et al. 2004) to remove bias, dark current and flat-field response signatures. The dithered images were combined using the MultiDrizzle package, which removes cosmic rays, and corrects the images for geometric distortion.

Photometry was performed on the drizzled images using the DAOPHOT package within IRAF. Stars were automatically detected with DAOFIND in the F475W band, with the detection threshold set at 4σ above the local background level; the detections were then forced on the I band image. The instrumental magnitude of each object in each filter was estimated via a PSF-fitting technique. A spatially variable PSF was computed for both the F475W and F814W images, using ~ 180 isolated stars in different positions on the images.

Selection criteria based on the shape of the objects have been applied to the photometric catalog to remove as many spurious detections, blended and/or extended objects as possible. We have considered the DAOPHOT “sharpness” parameter, which sets the intrinsic angular size of the objects, and selected only those with $-0.5 < \text{sharpness} < 0.5$ in both filters. These sharpness values allow us to reject spurious and extended objects without eliminating the bright stars. We emphasize that the FUV objects are only partially resolved in the ACS data: one WFC/ACS pixel corresponds to $0.05''$, which is ~ 1.5 pc at the distance of M81. Our final photometry is calibrated on the ACS VEGAMAG photometric system, with zero points adopted from Sirianni et al. (2005).

We have also measured the optical integrated flux at V of the FUV objects detected by GALEX by averaging the F475W and F814W images, and using the POLYPHOT routine in IRAF with the GALEX FUV contours, to determine V magnitudes in the AB system. Although the V magnitudes were measured in a pseudo V image, we included it in Table 1 since it is a standard magnitude provided in the literature.

Figure 6 shows the $F814W$ versus $F475W - F814W$ ($\sim B - I$) color-magnitude diagram (CMD) for all stars measured in the ACS field of view. The CMD shows a young and blue main sequence (MS) evolutionary phase, located at $F475W - F814W \sim -0.1$, with the brightest stars at $I \simeq 22.5$. A scarcely populated red plume is visible at $B - I > 1.5$ and extends up to $I \sim 21.0$. It is populated by red supergiants (RSGs) at the brighter magnitudes, and asymptotic giant branch stars (AGBs) at fainter luminosities. One of the most interesting features in the CMD is the diagonal strip of stars extending through $F475W - F814W \simeq 0.5$, $F814W \simeq 23$ and $F475W - F814W \simeq 1.5$, $F814W \simeq 27$. This strip is populated by stars at the hot edge of the helium core-burning phase. The concentration of stars in the range of colors $2 < F475W - F814W < 3$ and magnitudes $24 < F814W < 27$

corresponds to low mass ($M < 2.2 M_{\odot}$), older (age > 1 Gyr) stars in the red giant branch (RGB) evolutionary phase.

We used Padova isochrones for metallicity $Z = 0.001$, $Z = 0.004$ and $Z = 0.019$ (Fagotto et al. 1994a,b) to enable us to interpret the features visible in the CMD. Superimposed on Fig. 7 is the set of Padova isochrones for a metallicity $Z = 0.004$. We obtain this value for Z from the following considerations. For the old population, we can rule out metallicities as high as solar from the shape and broadening of the RGB. For the same reasons, we find that Z is unlikely to be < 0.004 . However we cannot exclude a slightly higher metallicity. The color and morphology of the blue edge of the blue loop evolutionary phase are sensitive to Z and age. We find that the colors of this structure can only be reproduced for $Z \approx 0.004$, assuming that star formation began ~ 300 Myr ago in Arp’s Loop and is continuing to the present. We cannot put strong constraints on Z for the young stellar population because there are not enough stars, and some of these stars may be multiple.

The youngest stars are concentrated where GALEX detected the FUV regions. We used GALEX isophotal contours to select stars within the FUV regions. CMDs corresponding to FUV objects #1 & #2, #5, #6, and #7 & #8 are shown in Fig. 7. A comparison with Padova isochrones indicates that the regions where the FUV objects are detected are mostly dominated by O and B stars with ages younger than 30 Myr.

Individual O stars are difficult to distinguish in CMDs based on optical filters because of their well known color degeneracy at these wavelengths. We also have the additional problem that any O stars in Arp’s Loop may be multiple objects (one WFC/ACS pixel corresponds to ~ 1.5 pc). To estimate the number of O stars in Arp’s Loop, we can use both the GALEX FUV fluxes and the nebular $H\alpha$ luminosity of Karachentsev & Kaisin (2007). We measure a total FUV flux of 2×10^{39} erg s $^{-1}$ (Table 1) and, using standard numbers, this is equivalent to ~ 50 O8V stars. This is an upper limit because we have neglected the contribution of B stars to the FUV flux. Karachentsev & Kaisin (2007) measure a total $H\alpha$ flux of 3.5×10^{-14} erg s $^{-1}$ cm $^{-2}$ giving $L(H\alpha) = 5.4 \times 10^{37}$ erg s $^{-1}$. Thus, assuming one O8V star has a photon ionizing luminosity Q_0 of 3×10^{48} s $^{-1}$ in the Lyman continuum (Smith, Norris & Crowther 2002), the observed $H\alpha$ flux is equivalent to 13 O8V stars. These rough estimates will increase if there is any internal extinction. Arp’s Loop is then equivalent to ~ 5 Orion nebulae, if we assume that the Orion Nebula has an $H\alpha$ luminosity of 10^{37} erg s $^{-1}$.

Fig.8 shows the spatial distribution of the main sequence and the RGB stars in the ACS image. It is clear that stars of both types are located in the same general areas of the image with only two exceptions, at (1400,1600) and (3400, 3400). These regions of the image have many MS stars and only a couple of RGBs are seen. The first region is not among the

GALEX sources, it is close to the bright star on the south-east side of Fig.3 and the other region corresponds to object #6.

In summary, we find both an old and a young stellar population in Arp’s Loop with a similar spatial distribution and a metallicity $Z \sim 0.004$. It is likely that the old stellar population was formed in the M82 and/or M81 galaxies and ejected into the intergalactic medium during a tidal passage ($\sim 200\text{--}300$ Myr ago), whereas the young stars detected by GALEX have formed since the encounter in the tidal debris.

4. Discussion

4.1. Star Formation in Tidal Debris

Observational evidence is accumulating that star formation often occurs in low gas density environments. Examples include the outer disks of galaxies (e.g. Ferguson et al. 1998, Thilker et al. 2005) and tidal tails (e.g. Saviane, Hibbard, & Rich 2004, Hibbard et al. 2005). The nearest example is the HI bridge between the Magellanic Clouds (see Demers & Battinelli 1998), located at a distance of 50–60 kpc which allows very detailed investigations of both its interstellar gas and stars. The bridge has a complex structure in HI with typical column densities of $10^{20}\text{--}10^{21} \text{ cm}^{-2}$ (Muller et al. 2003, 2004) and somewhat higher in smaller regions. The Harris (2007) optical survey confirms that stars along the Magellanic bridge not only formed in place but also formed in material that contains very few old red giant stars. Molecular line surveys (Mizuno et al. 2006) and follow-up searches for pre-main-sequence stars (Nishiyama et al. 2007) demonstrate that despite overall low HI column densities, the conditions necessary for star formation and young stellar candidates exist in some places along the western part of the bridge that extends from the wing of the Small Magellanic Cloud. The more diffuse Magellanic stream with $N(\text{HI}) \lesssim 3\text{--}5 \times 10^{20} \text{ cm}^{-2}$ (e.g. Brüns et al. 2005), however, is not known to contain any stars (Majewski et al. 1999).

At the other extreme, relatively intense star formation is detected in FUV images of more massive gas rich tidal tails (e.g. Hibbard et al. 2005 for the Antennae, and Neff et al. 2005 for NGC 7769/71, NGC 5713/19, Arp 295, and the NGC 520 system). In these cases, large HII regions, OB associations, and even super star clusters can form, especially in situations where the HI column densities are $N(\text{HI}) > 4 \times 10^{20} \text{ cm}^{-2}$ over large regions (Maybhate et al. 2007). Thus the tidal bridge between M81–M82 where Arp’s loop is located ($N(\text{HI}) \sim 5\text{--}30 \times 10^{20} \text{ cm}^{-2}$; Yun et al. 1994) appears to support star formation at rates which are intermediate between the extremely low levels seen in an object like the Magellanic bridge and very active tidal tails like those found in, for example, NGC4676 (“The Mice”;

de Grijs et al. 2003). This suggests that the tidal HI streams in the M81 system sit near the low end of a continuum of levels of star formation in gas-rich tidal matter.

Star formation requires the production of gravitationally bound molecular clouds. Since tidal streams normally are at most only mildly gravitationally unstable on large spatial scales, star formation is not expected to behave in the same way as in the inner disks of galaxies which exist on the edge of large scale gravitational instability (Kennicutt 1989). The possibility that collisions between gas clouds could lead to star formation in low density but gas-rich environments such as the Magellanic bridge was explored by Christodoulou et al. (1997). In their model, compression to the densities required to make bound molecular structures was accomplished through post-shock compression. This picture gained support as observations improved; e.g. Muller & Parker (2007) make a case for the Magellanic bridge being a prime example of star formation resulting from turbulence.

More recent investigations, such as that of Bergin et al. (2004) and Heitsch et al. (2006), include the effects of turbulence which can enhance density perturbations more readily leading to molecular regions that can collapse to make stars in lower velocity cloud collisions. In these models sufficient columns of HI must interact with speeds of $\geq 10 \text{ km s}^{-1}$ to produce local regions with $N(\text{HI}) \geq 10^{21} \text{ cm}^{-2}$ that are required to readily shield molecular gas from radiative dissociation. The basic idea of triggering star-formation by cloud collision in Arp’s Loop is consistent with the Yun (1999) model for this feature being a stream crossing zone and with the HI observations showing comparatively high $N(\text{HI})$ in a region with a substantial $\sim 30 \text{ km s}^{-1} \text{ kpc}^{-1}$ and complex velocity field (Rots & Shane 1975; Rots 1975; Yun et al. 1994).

Ongoing star formation in relatively diffuse structures, such as Arp’s Loop, is consistent with expectations for gas collisions and subsequent turbulence to lead to inefficient conversion of gas into stars in low density systems such as tidal tails. On the other hand, the younger star forming sites seem to be relatively normal objects with properties similar to the Orion Nebula. Here we find support for the expectation that once a gravitationally bound molecular cloud forms in a low density environment, its subsequent evolution is largely controlled by factors that only weakly depend on how the cloud was formed.

4.2. Connections with Intergalactic HII Regions and Tidal Dwarf Galaxies

The ages and locations of objects containing young stars indicate that self-gravitating substructures form within HI tidal material in a variety of interacting systems. This tidal matter from interacting galaxies is expected to remain bound to one of the galaxies. Much

of it will relatively quickly fall back into the galaxies, although some matter may remain detached for as long as a Hubble time. For example, according to Hibbard & Mihos (1995) $\sim 20\%$ of the tidal material of NGC7252, a well-known merger remnant, is likely to remain in the local intergalactic medium. Tidal optical features are also known to host “tidal dwarf galaxies” (TDGs) (e.g. Duc et al. 1997; Weilbacher et al. 2000; Knierman, et al. 2003; Bornaud et al. 2004). The eventual fate of the TDGs and the stars and metals that they produce remains unclear. For instance, the TDG-candidate found in the compact group HCG100 (de Mello et al. 2007) observed with GALEX has young (< 5 Myr) stellar populations and is located ~ 100 kpc away from the main galaxies. These systems therefore have the possibility to remain as independent objects over time scales of ≥ 1 Gyr.

The FUV objects in the M81 group are much closer to a large spiral than the HCG100 TDG, as they are only ~ 17 kpc in projected distance from M81 (nucleus) and ~ 15 kpc from the central region of the TDG-candidate, Holmberg IX. Besides being located closer to the parent galaxies than a long-lived TDG-candidate, the 8 FUV objects have much lower UV luminosities than the objects studied by de Mello et al. (2007) and Neff et al. (2005). As discussed in Sect. 3, their FUV luminosities are equivalent to ~ 50 late O stars. The fact that the M81 group is so close and that GALEX is sensitive to very low star-formation levels, $10^{-3} M_{\odot} \text{ yr}^{-1}$ (Salim et al. 2005), makes it possible to detect the Arp’s loop FUV objects. Are we then seeing a more diffuse example of star formation, as may be the case in the Magellanic bridge, or is the Arp’s loop region in an earlier evolutionary phase where star formation has not progressed far enough to produce a denser region? Increasing the stellar density is critical for this object to become a TDG (Mizuno et al. 2006). Better kinematic and baryonic mass density information are required to address this question.

It is also possible that the Arp’s loop FUV regions are analogs to the so-called ‘intergalactic HII’ regions of Mendes de Oliveira et al. (2004), Ryan-Weber et al. (2004) and Oosterloo et al. (2004). These objects seem to be similar to the HII regions in our Milky Way, but are located in regions with no optical connections to nearby galaxies. The fate of these type of objects and their importance in galaxy evolution and in the enrichment of the intergalactic medium are still debatable. These star-forming clumps can (1) remain as independent entities and grow to become TDGs by accreting more gas and forming more stars, (2) make star clusters that survive to live in the distant halos of their hosts or even become intergalactic objects, or (3) dissolve and not remain gravitationally bound yielding only very sparse star streams.

5. Conclusions

We have analyzed the UV and optical light within the H I bridge between M81 and M82 system and identified 8 FUV regions in an area known as Arp’s loop. Four of these objects were also detected in H α . High resolution ACS images show six of the regions in great detail and allow us to trace their star formation history. The synthetic CMD modeling shows the presence of a young population (< 10 Myr) together with an older component with ages > 1 Gyr. It is possible that these two populations are not related. In any case the young population must have formed “in situ” whereas the old population probably was formed in the M82 and/or M81 galaxies, and removed from their disks during a tidal passage ~ 200 – 300 Myr ago which also triggered star formation in the H I debris.

The FUV luminosities of the eight objects we detect are modest and typical of small clusters or associations of O and B stars. It is likely that these young stars have condensed recently from the tidally stripped gas from M81 and M82. The tidal bridge between M81–M82 appears to be intermediate between the very low levels of star formation seen in an object like the Magellanic bridge and very active tidal tails like those found in interacting galaxies such as the Mice and the Antennae. Ongoing star formation in relatively diffuse structures, such as Arp’s Loop, is consistent with expectations for gas collisions and subsequent turbulence to lead to inefficient conversion of gas into stars in low density systems such as tidal tails.

The fate of these star-forming clumps is not clear. They can grow to become TDGs, or make star clusters that survive to live in the distant halos of their hosts, or even become intergalactic objects. Finally, they may dissolve and not remain gravitationally bound, yielding only very sparse star streams. In any case, they will have a composite population of old and young stars formed in very different environments such as the M81/M82 disks and the tidal bridge. More observations of interacting systems similar to the M81 group will help establish the importance of these systems in galaxy evolution and in the enrichment of the intergalactic medium.

DFdM was funded by STScI grant-44185 and ES was funded by STScI GO grant-10248.07-A. JSG thanks the University of Wisconsin for partial support of this research.

GALEX is a NASA Small Explorer, launched in 2003 April. We gratefully acknowledge NASA’s support for construction, operation, and science analysis for the GALEX mission, developed in cooperation with the Centre National d’Etudes Spatiales of France and the Korean Ministry of Science and Technology.

This research has made use of the NASA/IPAC Extragalactic Database (NED) which

is operated by the Jet Propulsion Laboratory, California Institute of Technology, under contract with the National Aeronautics and Space Administration.

Facilities: HST (ACS/WFC), GALEX, WIYN.

REFERENCES

- Appleton, P.N., Davies, R.D., & Stephenson, R.J. 1981, MNRAS, 195, 327
- Arp, H. 1965, Science, 148, 363
- Bergin, E. A., Hartmann, L. W., Raymond, J. C., & Ballesteros-Paredes, J. 2004, ApJ, 612, 921
- Bertin, E., & Arnouts, S. 1996, A&AS, 117, 393
- Bournaud, F., Duc, P.-A., Amram, P., Combes, F., & Gach, J.-L. 2004, A&A, 425, 813
- Boyce, P.J. et al. 2001, ApJ, 560, L127
- Brüns, C., et al. 2005, A&A, 432, 45
- Christodoulou, D. M., Tohline, J. E., & Keenan, F. P. 1997, ApJ, 486, 810
- de Grijs, R. et al. 2003, NewA, 8, 155
- de Mello, D.F., Torres-Flores, S., & Mendes de Oliveira, C. 2007, AJ submitted
- de Mello, D.F., Leitherer, C., & Heckman, T.M. 2000, ApJ, 530, 251
- Demers, S., & Battinelli, P. 1998, AJ, 115, 154
- Duc, P.-A., & Mirabel, I.F. 1997, The Messenger 89, 14
- Efremov, Yu.N., Karachentsev, I.D., & Karachentseva, V.E. 1987, Sov. Astron. Lett., 12, 181
- Fagotto, F., Bressan, A., Bertelli, G., & Chiosi, C. 1994a, A&AS, 104, 365
- Fagotto, F., Bressan, A., Bertelli, G., & Chiosi, C. 1994b, A&AS, 105, 29
- Ferguson, A.M.N., Wyse, R.F.G., Gallagher, J. S., & Hunter, D. A. 1998, ApJ, 506, L19
- Freedman, W.L., et al. 1994, ApJ, 427, 628

- Gottesman, S.T., & Weliachew, L. 1975, *ApJ*, 195, 23
- Harris, J. 2007, *ApJ*, 658, 345
- Heitsch, F., Slyz, A. D., Devreindt, J. E. G., Hartmann, L. W., & Burkert, A. 2006, *ApJ*, 648, 1052
- Hibbard, J.E., & Mihos, J.C. 1995, *AJ*, 110, 140
- Hibbard, J.E., et al. 2005, *ApJ*, 619, L87
- Karachentsev, I.D., Kaisin, S.S. 2007, *AJ*, 133, 1883
- Kennicutt, R. C. Jr. 1989, *ApJ*, 344, 685
- Knierman, K.A., et al. 2003, *AJ*, 126, 1227
- Makarova, L.N. et al. 2002, *A&A*, 396, 473
- Majewski, S. R., Ostheimer, J. C., Kunkel, W. E., Johnston, K. V., Patterson, R. J., & Palma, C. 1999, *New Views of the Magellanic Clouds*, 190, 508
- Maybhate, A., et al. 2007 (arXiv:0707.3582)
- Mendes de Oliveira, C., Cypriano, E.S., Sodré, L. Jr, & Balkowski, C. 2004, *AJ*, 132, 570
- Mizuno, N., et al. 2006, *ApJ*, 643, 107
- Morrissey, P., et al. 2005, *ApJ*, 619, L7
- Muller, E., & Parker, Q. A. 2007, *Publications of the Astronomical Society of Australia*, 24, 69
- Muller, E., Staveley-Smith, L., Zealey, W., & Stanimirović, S. 2003, *MNRAS*, 339, 105
- Muller, E., Stanimirović, S., Rosolowsky, E., & Staveley-Smith, L. 2004, *ApJ*, 616, 845
- Neff, S.G., et al. 2005, *ApJ*, 619, L91
- Nishiyama, S., et al. 2007, *ApJ*, 658, 358
- Oosterloo, R., et al. 2004 in ‘Recycling Intergalactic and Interstellar Matter’ *IAUS 217*. Eds., P-A Duc, J. Braine, & E. Brinks, 486, 492
- Pavlovsky C., et al. 2004, “ACS Instrument Handbook”, Version 5.0, (Baltimore: STScI)

- Ryan-Weber, E.V., Meurer, G.R., Freeman, K.C., Putman, M.E., & Webster, R.L. 2004, *AJ*, 127, 1431
- Rots, A.H., 1975, *A&A* 45, 43
- Rots, A.H., Shane, W.W., 1975, *A&A* 45, 25
- Sabbi, E., et al. 2007 in preparation
- Salim, S., et al. 2005, *ApJ*, 619, L39
- Saviane, I., Hibbard, J. E., & Rich, R. M. 2004, *AJ*, 127, 660
- Schombert, J.M., Wallin, J.F. & Struck-Marcell, C. 1990, *AJ*, 99, 497
- Seibert et al. 2005, *ApJ* 619, L55
- Sirianni et al. 2005, *PASP*, 117, 1049
- Smith, L. J., Norris, R. P. F. & Crowther, P. A. 2002. *MNRAS*, 337, 1309
- Sun, W.-H., et al. 2005, *ApJ*, 630, L133
- Thilker, D. A. et al. 2005, *ApJ*, 619, L79
- van der Hulst, J.M. 1979, *A&A*, 75, 97
- Yun, M.S., Ho, P.T.P., & Lo, K.Y. 1994, *Nature*, 372, 530
- Yun, M.S., 1999, in: *IAU Symp. 186, Galaxy Interactions at Low and High Redshift*, ed. J.E. Barnes & D.B. Sanders (Dordrecht: Kluwer), 81
- Weilbacher, P. M., Duc, P.-A., Fritze v. Alvensleben, U., Martin, P., & Fricke, K. J. 200, *A&A*, 358, 819

Table 1. FUV sources

ID	RA	Dec	m_V	FUV	L_{FUV} (erg/s)	NUV	L_{NUV} (erg/s)
1+2	149.313562	69.278637	20.25 \pm 0.07	18.17 \pm 0.02	1.09E+039	19.46 \pm 0.02	6.48E+038
3	149.304548	69.273482		19.77 \pm 0.05	2.48E+038	21.17 \pm 0.06	1.34E+038
4	149.317475	69.273476		20.03 \pm 0.06	1.94E+038	21.13 \pm 0.04	1.40E+038
5	149.328273	69.273482	21.23 \pm 0.05	20.53 \pm 0.07	1.23E+038	20.78 \pm 0.05	1.92E+038
6	149.374412	69.266872	21.52 \pm 0.08	19.60 \pm 0.04	2.90E+038	20.45 \pm 0.04	2.61E+038
7	149.393938	69.294389	22.33 \pm 0.07	21.33 \pm 0.1	5.91E+037	22.23 \pm 0.09	5.06E+037
8	149.390473	69.296530	22.68 \pm 0.09	21.03 \pm 0.09	7.80E+037	21.95 \pm 0.08	6.52E+037

Note. — FUV magnitudes were obtained with SExtractor (Bertin & Arnouts 1996) Mag_auto in the AB system. m_V is the magnitude within the FUV contour. Galactic extinction corrections were done using Seibert et al. (2005) for FUV and NUV. Objects 1 and 2 are not resolved with GALEX and no deblending correction was applied.

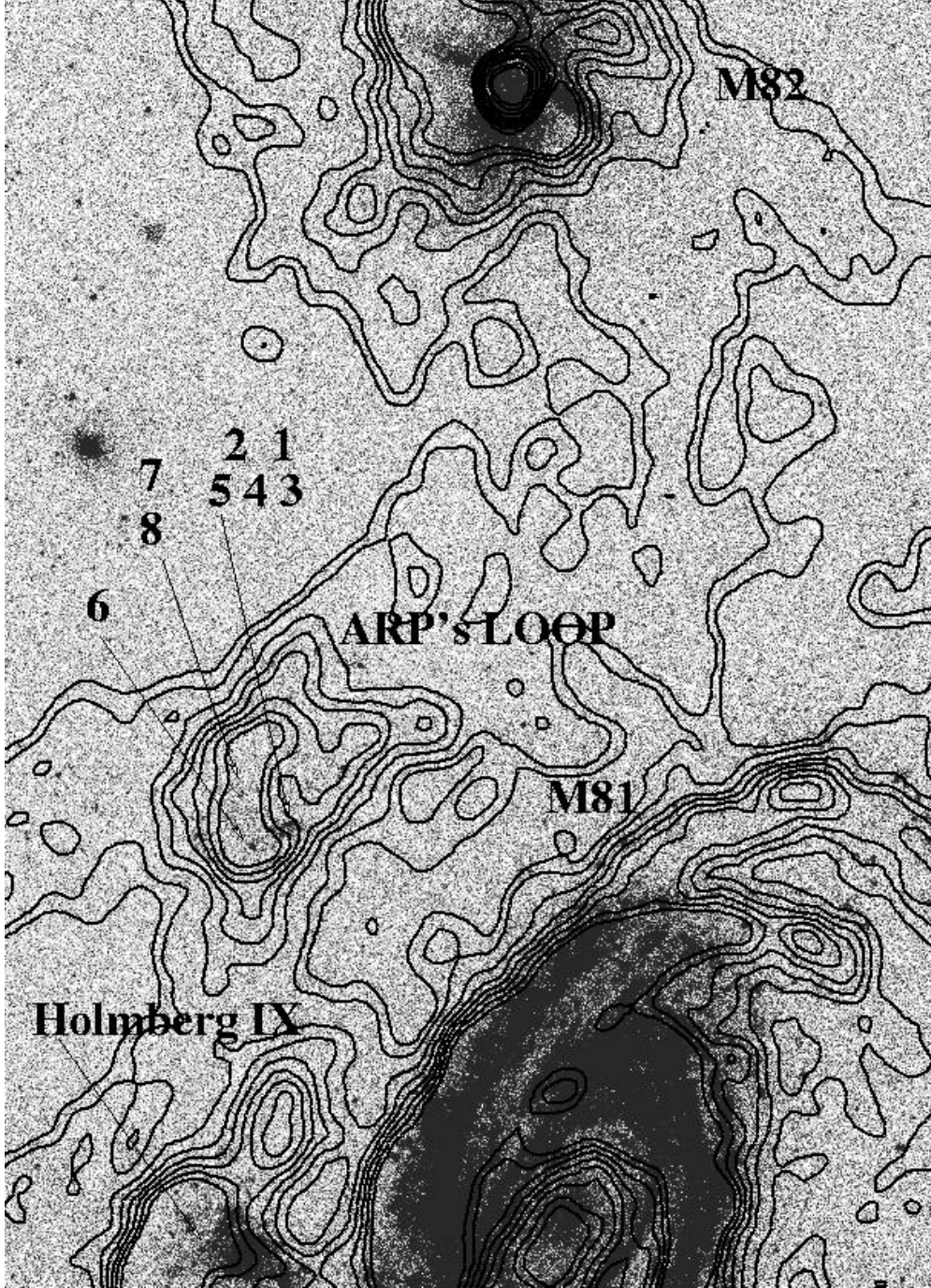


Fig. 1.— GALEX FUV image of the M81 and M82 region where FUV objects are detected. The contours in black are HI contours from Yun et al. (1994). FUV objects are numbered 1-8 and the general location of the region called Arp's loop is marked. North is to the top and East to the left, M81 is shown partially in the bottom of the image and M82 in the top of the image, Holmberg IX is to the east of M81, the cutout is $31.1' \times 42.6'$. HI contours adapted from Yun, Ho & Lo's Fig. 1 by permission from Macmillan Publishers Ltd: Nature, copyright (1994).

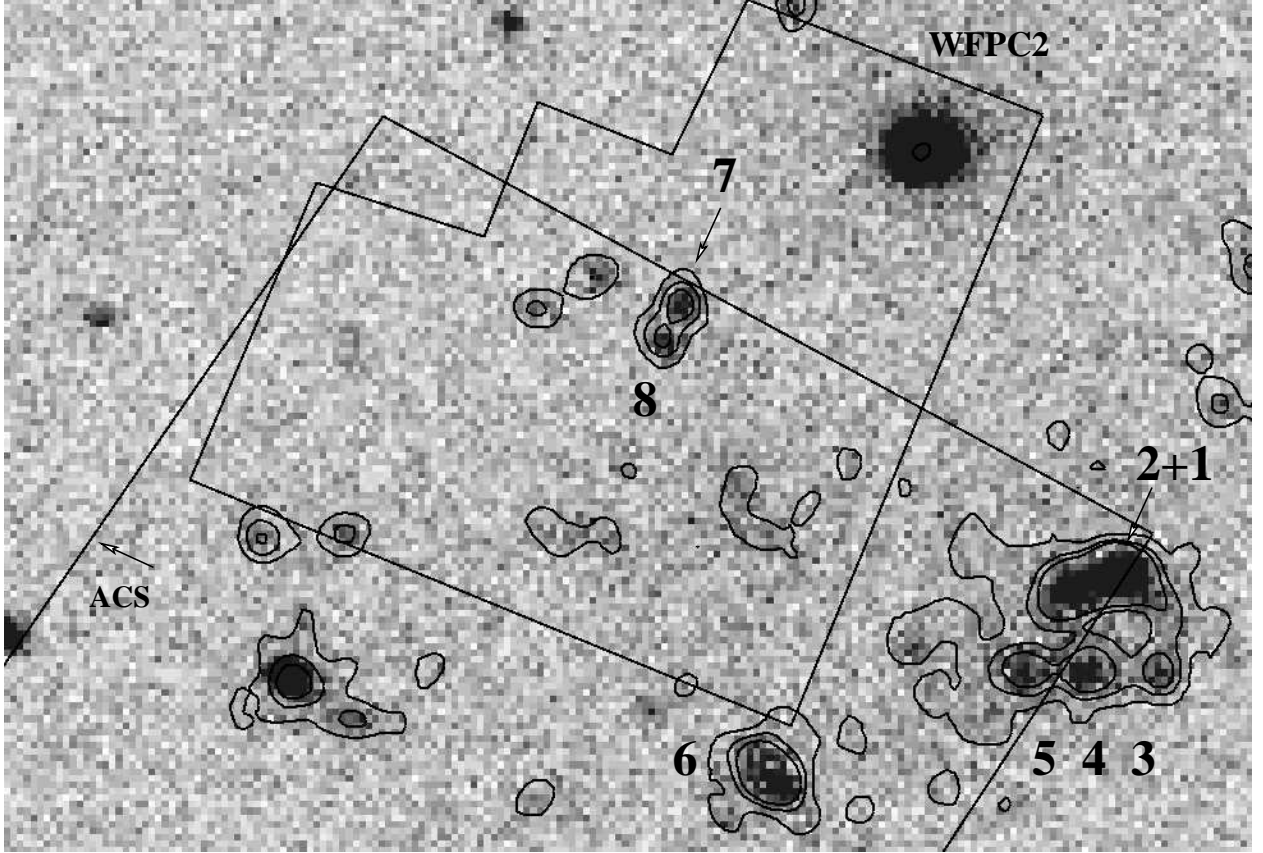


Fig. 2.— GALEX NUV image with FUV contours in black (contour levels are 0, 0.0006, 0.009 and 0.001 counts). The blue blobs numbered 1-8 in Fig. 1, the ACS footprint, and WFPC2 region used in Makarova et al. (2002) are marked. The cutout is $4.8' \times 3.2'$. North is to the top and East to the left.

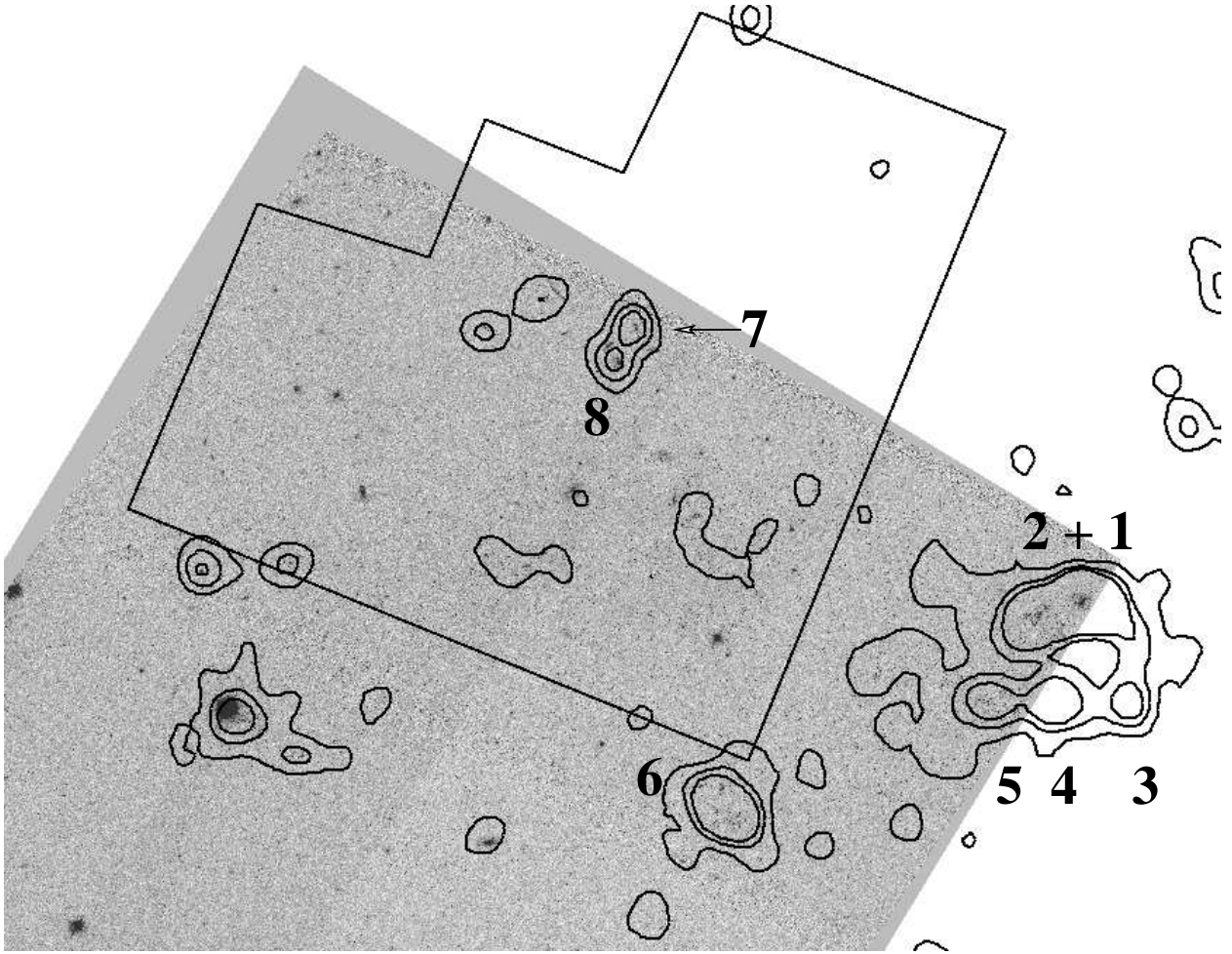


Fig. 3.— ACS/F475W image of the region where FUV objects are detected ($4.5' \times 3.3'$). GALEX FUV contours are shown in black. WFPC2 region used in Makarova et al. (2002) is marked. North is to the top and East to the left.

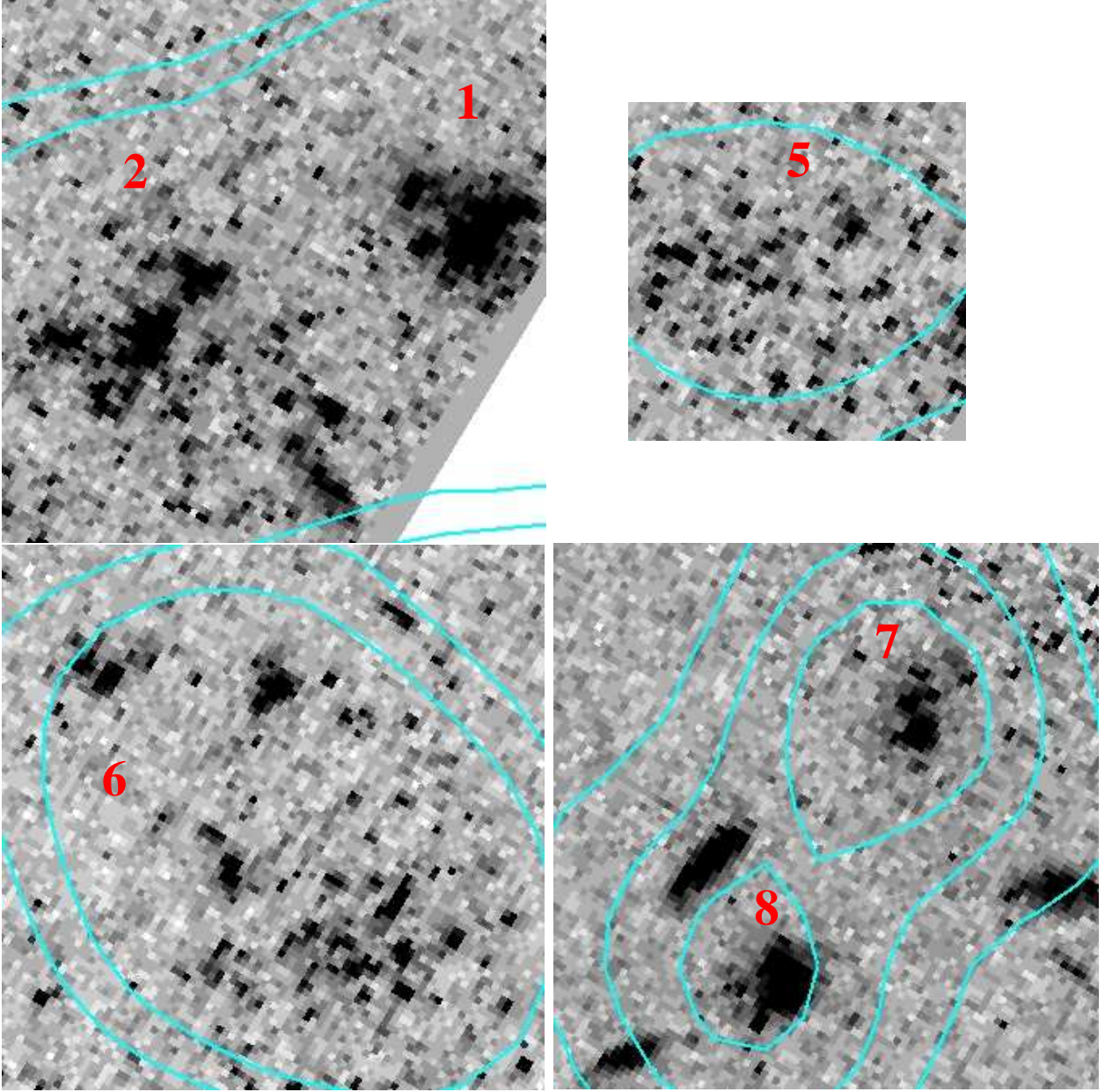


Fig. 4.— ACS/F475W image cutouts. Objects #1 and 2 are shown within a $16'' \times 16''$ box, objects #3 and 4 are outside the ACS pointing, object #5 is shown within a $10'' \times 10''$ box, object #6 is shown within a $16'' \times 16''$ box, objects #7 and 8 are shown within a $16'' \times 16''$ box. GALEX FUV contours are shown in cyan. North is to the top and East to the left.

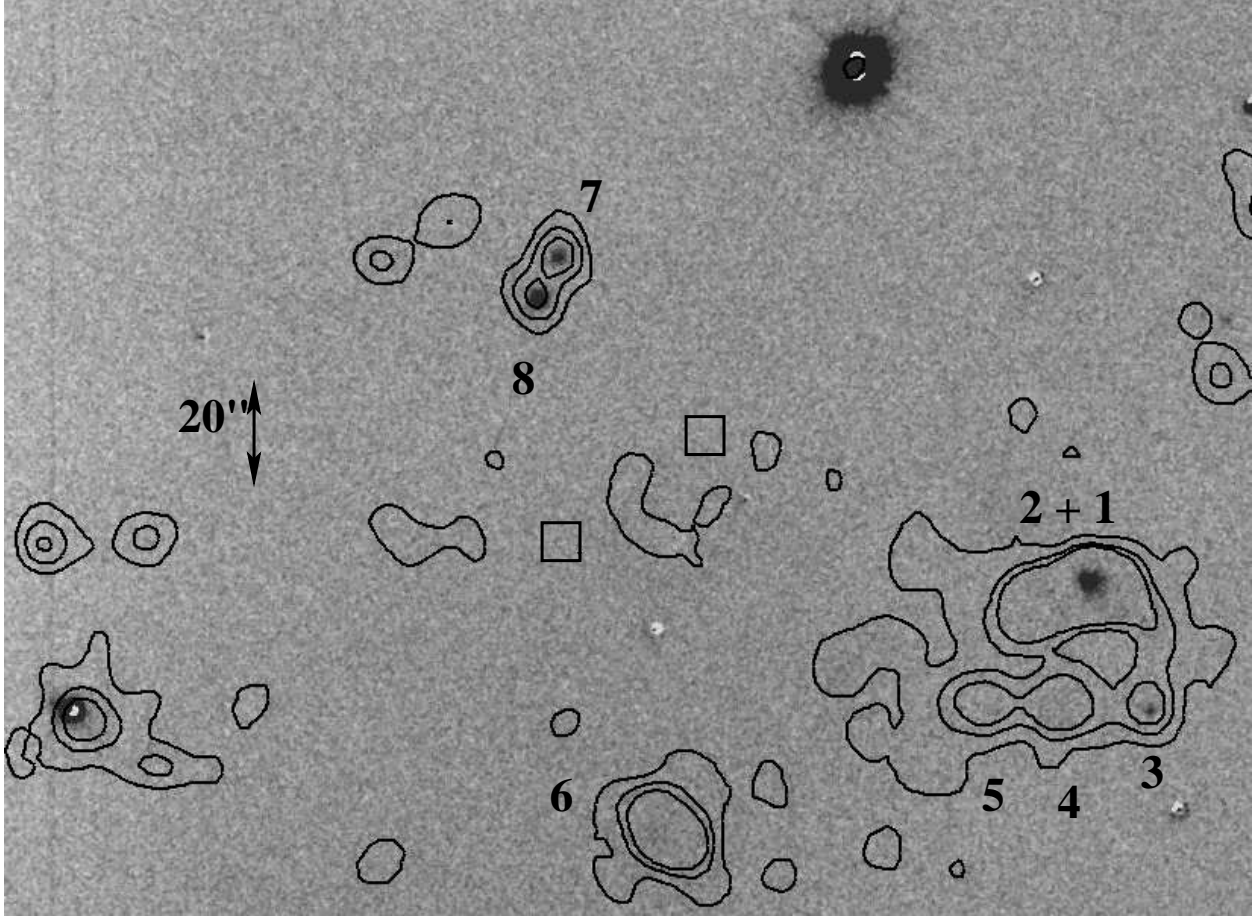


Fig. 5.— WIYN 3.5m telescope $H\alpha$ continuum subtracted (smoothed with a 5×5 median filter) image. The two boxes show the location of two objects detected by Karachentsev & Kaisin (2003) but not present in our data. GALEX FUV contours are shown in black. North is to the top and East to the left.

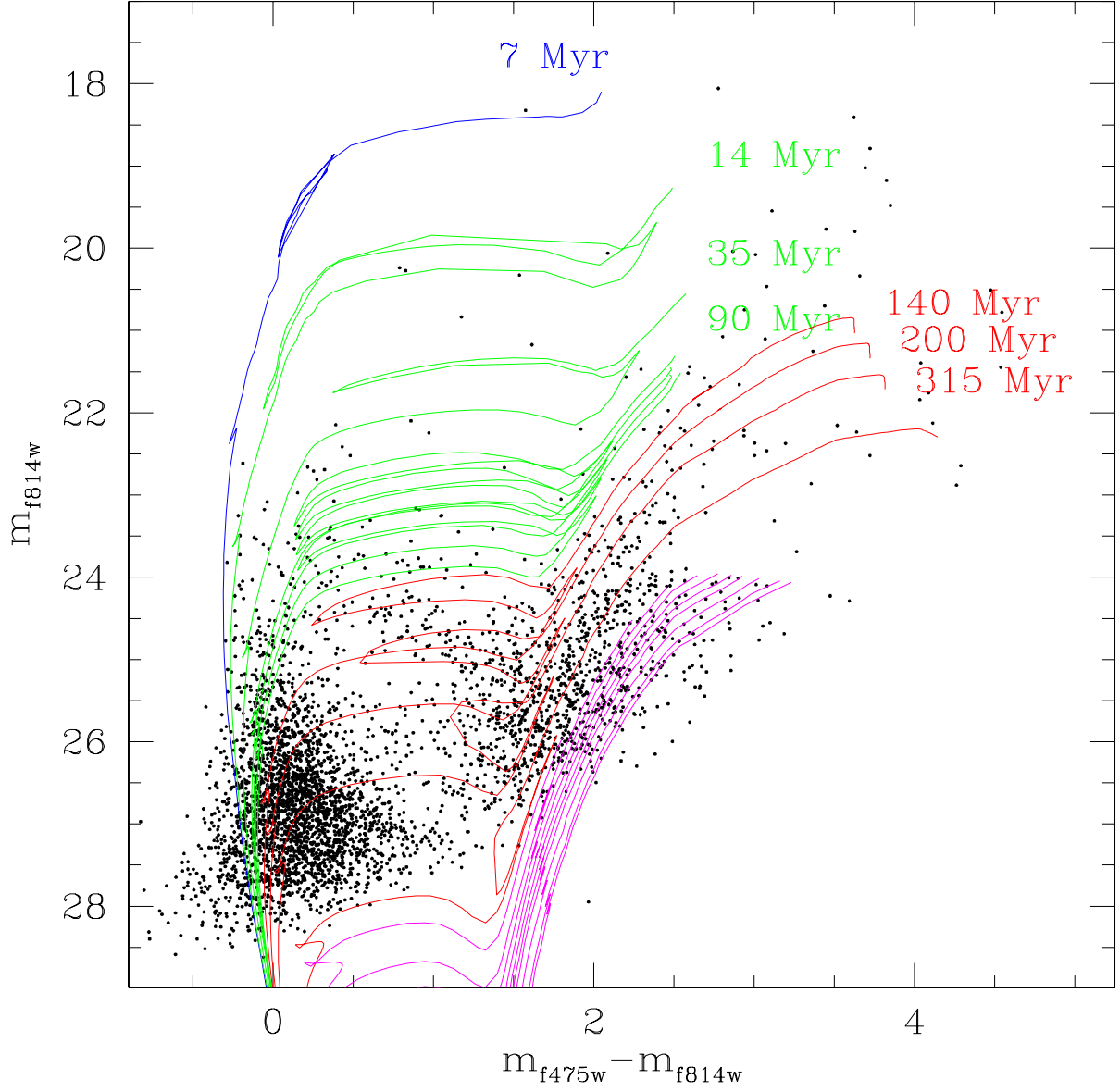


Fig. 6.— Color-magnitude diagram, $F814W$ versus $F475W - F814W$ ($\sim I$ versus $B - I$), of all stars measured in the ACS field of view. Superimposed on the CMD are Padova isochrones (Fagotto et al. 1994a,b), with a metallicity $Z=0.004$ and ages 7 Myr to 10 Gyr.

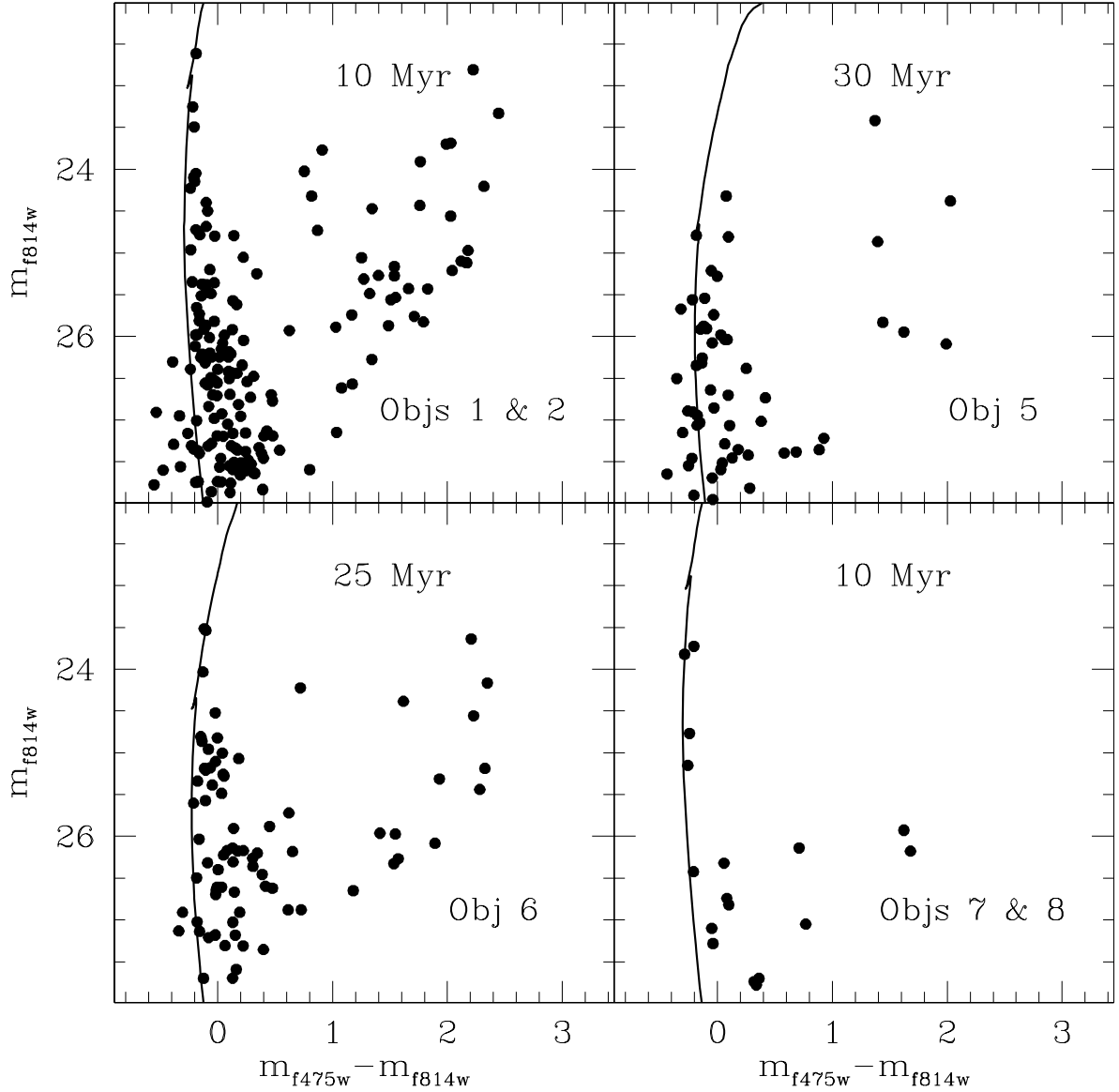


Fig. 7.— Color-magnitude diagram, $F814W$ versus $F475W - F814W$ ($\sim I$ versus $B - I$), of the FUV regions 1-8. Superimposed on the CMD are Padova isochrones (Fagotto et al. 1994a,b), with a metallicity $Z=0.004$ and ages 10 (regions # 1+ 2, and # 7+8) 25 (region # 6) and 30 Myr (region # 5).

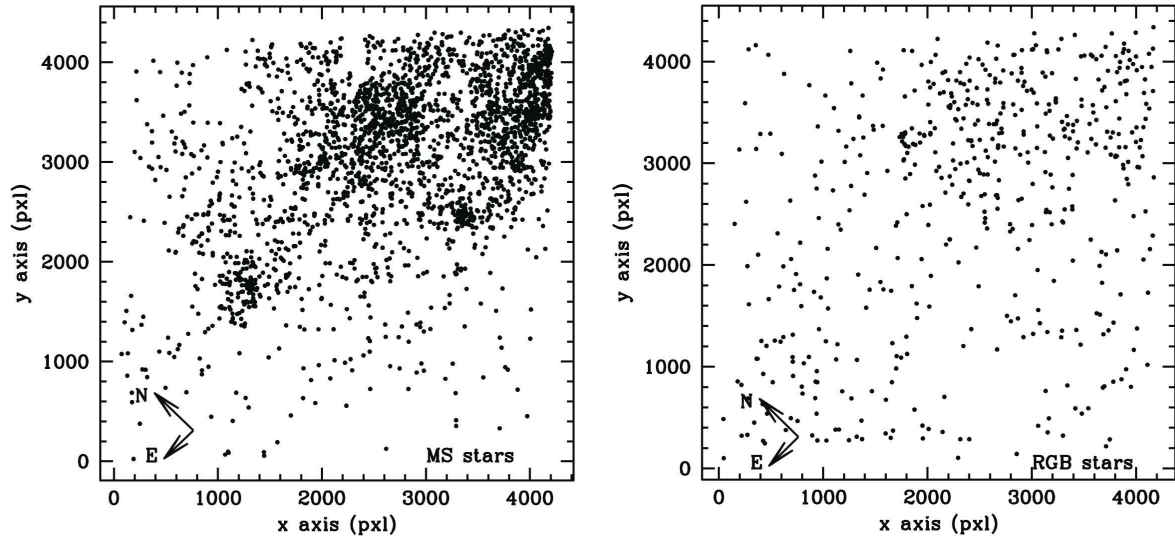


Fig. 8.— Spatial distribution of main sequence stars (left) and RGB stars (right) in the ACS image. Orientation N-E is shown in each plot.